Title

Lithium Charge Storage Mechanisms of Cross-Linked Triazine Networks and Their Porous Carbon Derivatives

Authors

See, Kimberly A
Hug, Stephan
Schwinghammer, Katharina
et al.

Publication Date

2015-05-15

DOI

10.1021/acs.chemmater.5b00772

Peer reviewed

Lithium charge storage mechanisms of cross-linked triazine networks and their porous carbon derivatives

Kimberly A. See,[†,‡] Stephan Hug,[§,^,ℌ] Katharina Schwinghammer,[§,^,ℌ] Margaret A. Lumley,[‡,∥] Yonghao Zheng,[∇] Jaya M. Nolt,[∥] Galen D. Stucky,[†,‡,∇] Fred Wudl,[∇] Bettina V. Lotsch,[*,§,^,ℌ] Ram Seshadri[*,†,‡,∥,∇]

[†]Mitsubishi Chemical – Center for Advanced Materials, University of California, Santa Barbara, CA 93106, USA
[‡]Department of Chemistry and Biochemistry, University of California, Santa Barbara, CA 93106, USA
[ℌ]Nanosystems Initiative Munich and Center for Nanoscience, Schellingstr. 4, 80799 München, Germany
[§]Department Chemie, Ludwig-Maximilans-Universität München, Butenandtstr. 5-13, 81377 München, Germany
[^]Max-Planck-Institut für Festkörperforschung, Heisenbergstr. 1, 70569 Stuttgart, Germany
[∥]Materials Research Laboratory, University of California, Santa Barbara, CA 93106, USA
[∇]Materials Department, University of California, Santa Barbara, CA 93106, USA.

Carbon nitride, energy storage, organic radicals, organic Li battery, covalent triazine frameworks, porous polymers

ABSTRACT: Redox active electrode materials derived from organic precursors are of interest for use as alternative cathodes in Li batteries due to the potential for their sustainable production from renewable resources. Here, a series of organic networks that either contain triazine units, or are derived from triazine-containing precursors are evaluated as cathodes versus Li metal anodes as possible active materials in Li batteries. The role of the molecular structure on the electrochemical performance is studied by comparing several materials prepared across a range of conditions allowing control over functionality and long range order. Well-defined structures in which the triazine unit persists in the final material exhibit very low capacities at voltages relevant for cathode materials (<10 mA.h g^{-1}). Relatively high, reversible capacity (around 150 mA.h g^{-1}), is in fact displayed by amorphous materials with little evidence of triazine functionality. This result directly contradicts previous suggestions that the triazine unit is responsible for charge storage in this family of materials. While the gently sloping discharge and charge profiles suggest a capacitive-type mechanism – further confirmed by the trend of increasing capacity with increasing surface area – electron paramagnetic resonance spectroscopy studies show that the materials exhibiting higher capacities also display larger signals, potentially implicating unpaired spins in a charge storage mechanism that could involve charge transfer.

1. INTRODUCTION

Electrical energy storage materials largely utilize non-renewable, and relatively scarce elements such as Co in the canonical Li-ion battery cathode $LiCoO_2$.[1] Organic materials derived from renewable precursors are desirable replacement charge storage materials since they can be prepared in a sustainable manner using highly abundant elements obtained from renewable resources. Such materials do not suffer issues of scarcity or geopolitical pressures. It is not surprising therefore, that redox active organic materials suitable as battery or supercapacitor electrodes have been recently gaining interest.[2]

Redox active organic materials include small molecules, polymeric materials, and networks. Early work on organic materials for Li battery applications focused on carbonyl groups in polyoxocyclohexanes both as small molecules[3,4] and incorporated into polymers,[5] or in dicarboxylates[6] and ethoxycarbonyl-based materials.[7] Other functional groups have been explored as possible electrodes for secondary batteries such as organosulfur compounds which utilize the reversible reduction of disulfide bonds[8] in dimeric organodisulfides,[9] disulfides along the backbone of polymeric materials,[10] disulfides attached to the backbone of polymeric materials,[11] or polymeric materials containing polysulfide bonds.[12]

Organic free radical compounds have also been known to reversibly store electrons in Li batteries. Very stable oxygen-centered radical species such as nitroxide radicals can exhibit both n- and p-doped states by either acting as an oxidant by accepting an electron to pair the unpaired radical or acting as a reductant by donating the unpaired electron.[13,14] Similarly, it was recently suggested that rigid networks containing triazine moieties, termed amorphous covalent triazine-based frameworks (CTF), can also exhibit bipolar states to achieve reversible

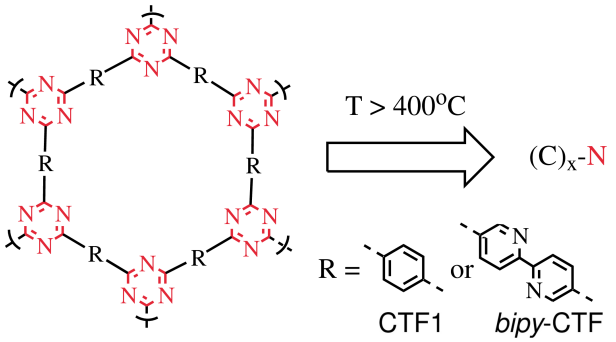

Figure 1. The covalent triazine-based frameworks, or CTFs, contain 1,3,5-triazine moieties bridged by rigid, conjugated units such as phenylene (CTF1) and 2,2'-bipyridyl (*bipy*-CTF). CTFs are more rigid and their structure and functionality can be modulated depending on the preparation temperature. When prepared above 400°C, the CTF materials no longer exhibit well-defined triazine moieties and exhibit amorphous carbon character with N-heteroatoms.

capacities in Li batteries up to about 150 mA.h g^{-1} via a similar mechanism in which the triazine unit can be both n- and p-doped.[15]

In an effort to expand on the idea of charge storage using triazine-based materials, we describe the effect of the structure and preparation conditions of a few triazine-based materials on their charge storage capabilities. This structural dependence gives insight into the mechanism of charge storage. Covalent triazine-based frameworks (CTF) that contain 1,3,5-triazine bridged by rigid, conjugated linkers such as *para*-phenylene or 2,2'-bipyridyl are discussed (Figure 1). When prepared above 400°C, the material no longer contains triazine units and instead consists of an amorphous C with N heteroatoms. The CTF materials were prepared at a variety of temperatures in order to elucidate the effect of long range order on the electrochemical performance. Through this in-depth study, we find that the triazine unit is not the responsible party for charge storage and instead, the materials must be prepared above the temperature at which triazine is stable in order to achieve amorphous carbons with relatively high gravimetric capacity.

CTFs have been evaluated in half cells in both Li-based systems[15] and Na-based systems[16] and even in an all-organic cell for both Li and Na batteries.[17] CTFs prepared at slightly higher temperatures were also evaluated as supercapacitor electrodes.[18] Here, we study similar materials with an emphasis on evaluating the cell performance of CTFs with different linkers, namely phenylene (CTF1) and 2,2'-bipyridyl (*bipy*-CTF), see Figure 1 for idealized structures, and prepared at various temperature. These materials are prepared from a *para*-dicyanobenzene[19] or 5,5'-dicyano-2,2'-bipyridine[20] precursors ionothermally in a $ZnCl_2$ melt, as described previously, with various equivalents of $ZnCl_2$ and at various temperatures.

By evaluating this wide range of materials prepared from 1,3,5-triazine containing precursors, we have determined that the triazine unit itself is not involved in charge storage through bipolar states as previously hypothesized.[15] Instead, we find that the CTF networks containing well-defined triazine units show very low capacity in Li cells. CTF materials prepared at higher temperatures form N-containing amorphous carbons with ill-defined, amorphous structures and exhibit much higher capacities when cycled in a Li half-cell. The is not surprising since similar N-containing porous carbons have been explored previously for application in supercapacitors.[18,21] Capacitive-like discharge and charge profiles are observed for amorphous materials and the materials' capacity trends with surface area, further suggesting a capacitive mechanism. Interestingly, the *bipy*-CTF and CTF1 materials exhibiting the largest capacity also have a large concentration of unpaired spins that may be involved in the charge storage mechanism. To confirm this hypothesis, well-defined poly(triazine imide) materials (PTI) that contain a high degree of triazine functionality and no unpaired spins are shown to be electrochemically inactive.

2. EXPERIMENTAL DETAILS

Preparation of CTF materials: The covalent triazine frameworks (CTF) were prepared in a $ZnCl_2$ melt at temperatures between 400°C and 600°C using either *para*-dicyanobenzene[19] (CTF1 networks) or 5,5'-dicyano-2,2'-bipyridine[20] (*bipy*-CTF networks) precursors. In a typical synthesis a Duran ampoule (1.5 x 12 cm) was charged with the dinitrile (500 mg) and $ZnCl_2$ (1-10 equivalents, see Table 1) in a glove box. The ampoule was flame sealed under vacuum and placed in a tube furnace. The ampoule was heated to temperatures between 400°C - 600°C and subsequently allowed to cool to ambient temperature. The ampoule was opened and its content ground thoroughly. The crude product was stirred in H_2O (75 mL) for 1 h, filtered, and washed with 1 M HCl (2 × 75 mL). The CTF was stirred at 90°C in 1 M HCl (75 mL) over night, filtered, and subsequently washed with 1 M HCl (3 × 75 mL), H_2O (12 × 75 mL), THF (2 × 75 mL), and dichloromethane (1 × 75 mL). Finally, the powder was dried overnight in a desiccator. The materials CTF1-400-1 and CTF1-400-10 are analogous to the crystalline CTF-1 and amorphous CTF-1 (ACTF-1), respectively, presented by Sakaushi et al.[15]

Materials characterization: Argon sorption measurements were performed at 87 K with an Autosorb-iQ surface analyzer (Quantachrome Instruments, USA). Samples were outgassed in vacuum at 150°C for 6-12 h to remove all guests. For BET calculations, pressure ranges of the Ar isotherms were chosen with the help of the BET Assistant in the ASiQwin software. In accordance with the ISO recommendations multipoint BET tags equal or below the maximum in $V \times (1 - P/P_0)$ were chosen. Fourier transformed infrared (FTIR) spectroscopy measurements were carried out on a Perkin Elmer Spectrum BX II (Perkin Elmer, USA) with an attenuated total reflectance unit. Powder X-ray diffraction (XRD) was measured on a BRUKER D8 Avance (Bruker AXS, USA) in Bragg-Brentano geometry. Elemental analysis (EA) was carried out with an Elementarvario EL (Elementar Analysensysteme, Germany). Solid state electron paramagnetic resonance (EPR) experiments were carried out on weighed

powders of the materials in sealed quartz capillary tubes inside 0.4 mm quartz EPR tubes. The spectra were recorded on a X-band (≈9 GHz) Bruker EMX spectrometer operating at 100 kHz field modulation, 2.0 μW (20 mW for CTF1-500) microwave power and fitted with a high sensitivity cavity. Cross polarization magic angle spinning (CP-MAS) solid-state nuclear magnetic resonance (ssNMR) spectra were recorded at ambient temperature on a BRUKER DSX500 Avance NMR spectrometer (Bruker Biospin, Germany) with an external magnetic field of 11.75 T. The operating frequencies are 500.1 MHz and 125.7 MHz for ^{1}H and ^{13}C, respectively, and the spectra were referenced relative to TMS. The samples were measured with a delay time of 1 s and a pulse length of 2.5 μs. The samples were contained either in 2.5 mm or 4 mm ZrO_2 rotors spinning at 20 kHz.

Table 1. Summary of preparation conditions for the covalent triazine-frameworks and their surface areas and C/N ratios.

	Eq. $ZnCl_2$	Syn. Temp. (°C)	Surface area ($m^2\ g^{-1}$)*	C/N ratio**
CTF1-400-1	1	400	610	3.77
CTF1-400-10	10	400	496	4.81
CTF1-500	5	500	1830	6.17
CTF1-600	5	600	2557	7.63
bipy-CTF-400	5	400	590	2.88
bipy-CTF-500	5	500	1680	3.85
bipy-CTF-600	5	600	2815	4.96

*BET surface area calculated from N_2 sorption isotherms
**C/N ratio is the ratio between the wt% of C/N calculated from elemental compositions as measured by elemental analysis. The full elemental analysis can be found in Table S1.

Electrochemical experiments were performed in loose powder Swagelok® cells with a Li foil anode, 1 M $LiPF_6$ in ethylene carbonate/dimethyl carbonate (EC/DMC) electrolyte (1/1, v/v), and a Whatman glass filter dryer (GFD) separator. The GFD separators were dried at 70°C under vacuum overnight prior to loading into the glove box. Composite powders were prepared by hand grinding the active materials with Super P® carbon additive at a 1:1 ratio for the CTF materials, and at 2:3 ratio for the PTI materials. The total mass loading of the composites was held constant at 10 mg. When compressed by hand in a Swagelok cell to a disc with a diameter of roughly 9 mm, the areal mass loading of the active material is in the 1:1 (active:carbon) composites is 8 mg cm^{-2} and 6 mg cm^{-2} for the composites prepared at a ratio of 2:3. The powders were then dried under vacuum overnight at 70°C prior to cell preparation. All cells were prepared in an Ar glove box. Galvanostatic cycling experiments and electrochemical impedance spectroscopy were done on a Bio–Logic Variable Multichannel Potentiostat at room temperature. The electrochemical impedance spectroscopy was performed before and after cell cycling (charged state) with a sinus amplitude of 100 mV from 1000 kHz to 10 mHz. Galvanostatic experiments were conducted at 0.1 A g^{-1} from 1.5 V to 4.5 V (vs. Li) starting firstly with discharge. All specific capacities are reported per gram of the active material, and not the total electrode mass.

3. RESULTS AND DISCUSSION

Two types of triazine-based materials bridged by rigid linkers, *para*-phenylene (CTF1)[19] and bipyridyl *(bipy*-CTF),[20] prepared at various temperatures were evaluated as electrodes in order to correlate the electrochemical performance to the surface area and structure (Table 1). Triazine-containing materials with rigid linkers are known to create porous organic networks with high surface areas[22] which would allow for increased electrolyte access to the material and greater charge storage capabilities. The structures of these materials are not well-defined so it is important to understand how the structure and network change with increasing preparation temperature and $ZnCl_2$ equivalents.

The CTF1 materials will be discussed first. In order to understand the long range and local order in the materials, IR and CP-MAS ^{13}C ssNMR spectra as well as XRD patterns were measured for each material (Figure 2). The only material that shows sharp 1,3,5-triazine stretches (expected at 1550 cm^{-1} and 1410 cm^{-1}) in the IR spectra is CTF1-400-1 (Figure 2a). Additionally, CTF1-400-1 is the only material in this series with long range order as evidenced by the two broad reflections in the XRD pattern, likely due to the sheet-like structure proposed by Kuhn et al.[19] Increasing the $ZnCl_2$ equivalents[19] or increasing the preparation temperature above 400°C results in reduced local order, causing broadened signals in the FTIR spectra, and reduced long range order, as evidenced by the absence of reflections in the XRD patterns (Figure 2). MAS ^{13}C ssNMR can give more insight into the short range order of the materials. The CTF1-400-1 spectrum (Figure 2c) shows a sharp resonance at 170 ppm correlated to C in the triazine ring. The sharp resonances at 138 ppm and 128 ppm belong to the C in the phenylene ring. The resonance at 116 ppm in the CTF1-400-1 spectrum suggests residues of nitrile groups although there is no indication of such in the FTIR. As the preparation temperature is increased, the 170 ppm peak vanishes indicating destruction of the triazine unit. Additionally, the phenylene peaks broaden significantly indicating disorder in the aromatic rings to an amorphous carbon. In short, CTF1-400-1 is the only material in which the schematic in Figure 1 is partially representative. CTF1-400-10, CTF1-500 and CTF1-600 show no evidence of triazine units and are best described as an amorphous carbon with the inclusion of N heteroatoms. Increasing the preparation temperature results in higher surface areas and increased C/N ratios presumably due to the decomposition of the triazine and liberation of N_2 (Table 1).

The electrochemical performance of the CTF1 materials was evaluated in a composite electrode with conductive carbon additive vs. a Li metal anode in 1 M $LiPF_6$ EC/DMC electrolyte. The CTF1-400-1 exhibits much lower reversible capacities (23 ± 10 mA.h g^{-1} at the 100th cycle) when cycled in a Li half-cell compared to the other

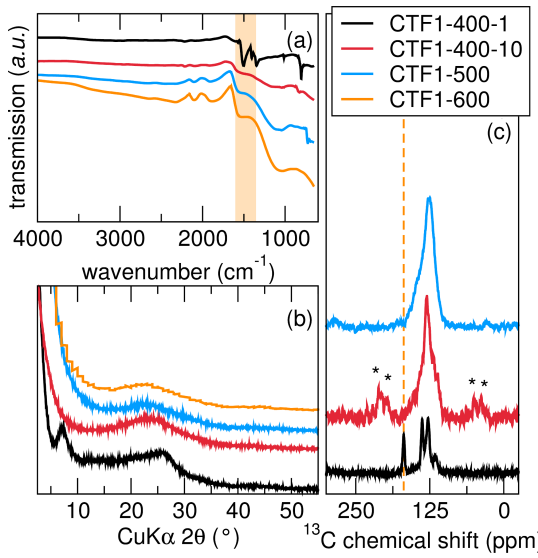

Figure 2. Characterization of the short and long range order in the CTF1 materials with (a) FTIR spectroscopy, (b) XRD, and (c) CP-MAS ^{13}C ssNMR. The wavenumber range in which triazine stretches are expected is highlighted by the orange box in (a) and the resonance of ^{13}C in the triazine ring is highlighted by the dashed line in (c). Due to the extent of carbonization of CTF1-600, a ^{13}C NMR spectrum was unable to be acquired.

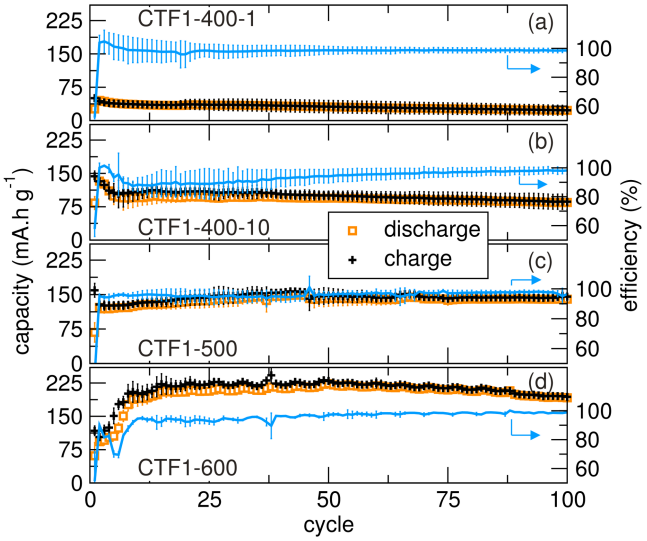

Figure 3. Discharge and charge capacities normalized per gram of active material and the Coulombic efficiency of the CTF materials over 100 cycles. The electrodes are 50% active with 50% Super P® and are cycled at 0.1 A g^{-1} in 1 M $LiPF_6$ EC/DMC at room temperature. The average of three replicate cells is shown with the standard deviation represented by error bars.

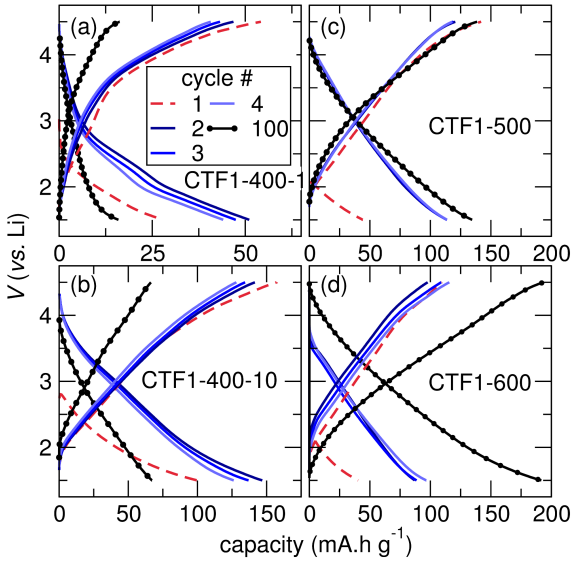

Figure 4. Discharge and charge profiles of the CTF1 materials with phenylene linker precursors cycled at 0.1 A g^{-1}. (a) CTF1-400-1 is a relatively well-defined material that exhibits low reversible capacities. (b) Higher equivalents of $ZnCl_2$ or (c, d) higher preparation temperatures destroys the triazine leaving an amorphous carbon with N heteroatoms and allows for the highest reversible capacities.

materials in the CTF1 family (Figure 3). Three replicate cells were cycled and the average capacity is plotted in Figure 3 along with the standard deviation, represented by the error bars. CTF1-400-10, which has a similar surface area to CTF1-400-1, exhibits a much higher reversible capacity (84 ± 15 mA.h g^{-1} at the 100th cycle). The difference between the two materials lies in the structure. CTF1-400-1 shows evidence of local and long range order, but CTF1-400-10 is an amorphous carbon with no long or short range order. In fact, the only materials that have substantial reversible capacities are amorphous carbons with N heteroatoms and no evidence of triazine units. Another interesting feature is that the capacity does not scale with surface area for this family of materials. Although CTF1-500 and CTF1-600 are much higher surface area materials compared to CTF1-400-10 (Table 1), all three materials exhibit similar reversible capacities. For all materials except CTF1-400-1, there is a low first discharge capacity which increases immediately to a relatively steady, reversible capacity thereafter. CFT1-600 exhibits a longer "equilibrating" period during which the capacity gradually increases to its steady reversible capacity. This type of behavior could be due to a swelling of the material as the cell is cycled allowing for more active material to be accessed. The capacity then begins to slightly fade likely caused by changes in morphology of the composite electrode resulting in degraded connectivity of the particle network. Capacity retention is enhanced for materials that are prepared at higher temperatures with CTF1-600 exhibiting the highest capacity at 100 cycles (143 mA.h g^{-1}). The CTF1-600 is the most amorphous in nature which facilitates charge storage. CTF1-600 most closely resembles the amorphous carbons known to be great capacitor materials.[18,21]

The shape of the discharge and charge profiles is very similar for all CTF1 materials (Figure 4). The gently sloping profile suggests a capacitive charge storage mechanism with negligible Faradaic activity. This is confirmed by the lack of peaks in the differential capacity curves for the CTF1 materials. CTF1-400-1 exhibits some kinks in the

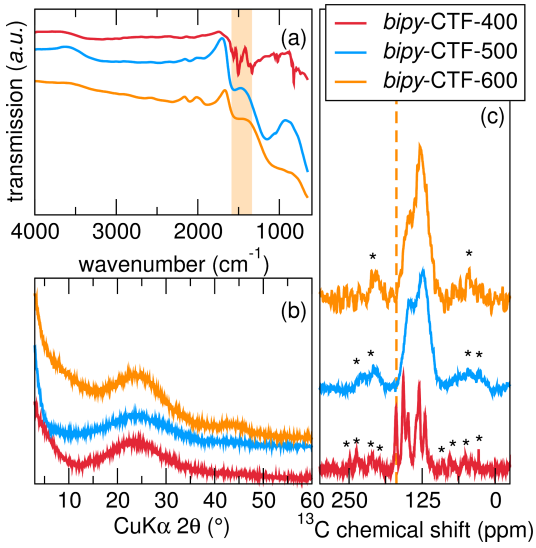

Figure 5. Characterization of the short range and long range order in the *bipy*-CTF materials with (a) FTIR spectroscopy, (b) XRD, and (c) MAS ^{13}C NMR. The wavenumber range in which triazine stretches are expected is highlighted by the orange box in (a) and the ^{13}C resonance of C in the triazine ring is highlighted by the dashed line in (c).

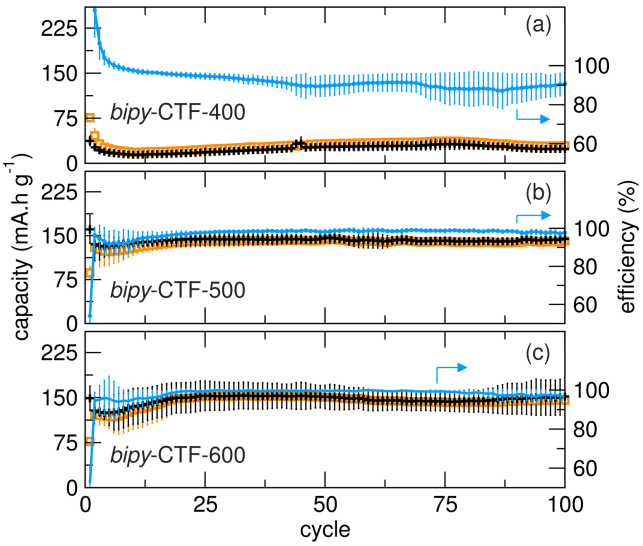

Figure 6. Discharge and charge capacities normalized per gram of active material and the Coulombic efficiency of the *bipy*-CTF materials over 100 cycles. The electrodes are 50% active with 50% Super P and are cycled at 0.1 A g^{-1} in 1 M $LiPF_6$ EC/DMC at room temperature. The average of three replicate cells is shown with the standard deviation represented by error bars.

discharge and charge profile which manifests as two broad peaks in the differential capacity curve around 2.8 V (vs. Li) and 2.0 V (vs. Li). Although these peaks are present during the initial cycles, the capacity is very low and the peaks disappear in subsequent cycles. Similar characteristics are observed when the cell is cycled at near-equilibrium conditions in a galvanostatic intermittent titration technique (GITT) experiment suggesting that the behavior at 0.1 A g^{-1} is indicative of equilibrium behavior. More details on the GITT and differential capacity curves can be found in the supplementary information. The cells were charged up to 4.5 V, which is approaching the limit of the electrochemical window of the carbonate electrolytes. However, there is no evidence of electrolyte decomposition that would manifest as a plateau at high potentials. The discharge and charge profiles for the CTF1 materials look capacitive, similar to those reported by Sakaushi et al.[15]

Triazine units bridged by 2,2'-birpyridyl moieties were also explored, termed *bipy*-CTF (see Figure 1 for an idealized structure). These materials exhibit very similar characteristics to the CTF1 materials in that*bipy*-CTF-400, prepared at 400°C, is the only material in this series that exhibits triazine signatures in the FTIR spectra and shows the characteristic ^{13}C signal in the NMR for C in the triazine ring (Figure 5a). Again, above 400°C, the triazine units are destroyed. The *bipy*-CTF-400 material shows no evidence for long range order in the XRD (Figure 5b) allowing for a comparison of an amorphous material which contains triazine (*bipy*-CTF-400), compared to CTF1-400-1 which has defined triazine units and moderate long range order. *bipy*-CTF materials prepared at higher temperatures are also amorphous, similar to *bipy*-CTF-400. Higher temperatures again result in higher surface area materials with lower N content (Table 1).

The same trends that relate the electrochemical performance and structure in the CTF1 materials hold true for the *bipy*-CTF materials. The one material in the series that shows distinct evidence of triazine in the spectroscopy, *bipy*-CTF-400, exhibits rather low reversible capacities (29 ± 6 mA.h g^{-1} at the 100th cycle). The materials prepared at 500°C and 600°C exhibit capacities of 141 ± 4 mA.h g^{-1} and 146 ± 25 mA.h g^{-1}, respectively, which is about 5 times higher than that of the *bipy*-CTF-400. The discharge profiles and measured capacities of the *bipy*-CTF materials are very similar to the CTF1 materials except *bipy*-CTF-400, which shows reversible Faradaic activity, but at a much lower capacity. This reversible Faradaic activity can be easily seen as two broad peaks in the differential capacity curve, which is in contrast to the amorphous materials that display no peaks suggesting capacitive behavior. The same plateaus are observed when the cell is cycled at near-equilibrium conditions. Details of the GITT and differential capacity curves can be found in the supplementary information. In order to determine the voltage dependence of the Faradaic processes, *bipy*-CTF-400 was also cycled between 1 V – 3 V (vs. Li) to determine if more substantial capacities can be achieved at lower potentials. The first discharge capacity increases, probably due to some electrolyte decomposition to form a solid electrolyte interphase (SEI) on the carbon additive,[23,24] however, the following capacities drop to magnitudes similar to the values measured when discharged to 1.5 V (vs. Li). The capacitive mechanism that is apparent in the materials prepared at higher temperatures does not seem to be present in *bipy*-CTF-400 due to the short range order and lack of amorphous carbon nature. *bipy*-CTF-500 and -600 exhibit high, reversible capacities and stable

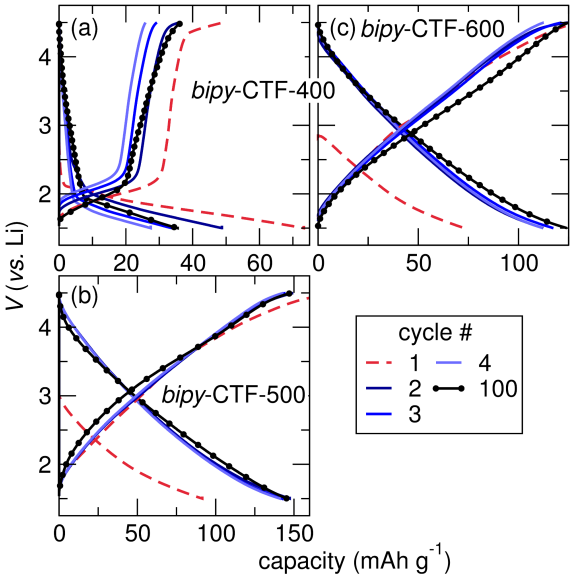

Figure 7. Discharge and charge profiles of the *bipy*-CTF materials cycled at 0.1 A g^{-1}. (a) *bipy*-CTF-400 exhibits low reversible capacities. (b, c) Higher preparation temperatures result in materials with highest reversible capacities.

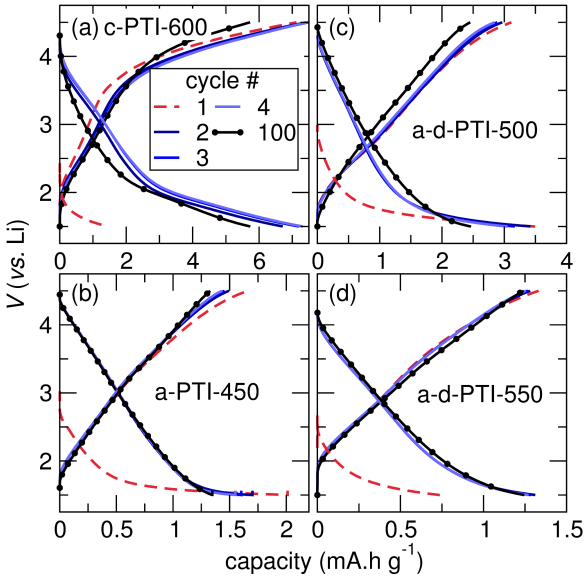

Figure 8. Discharge and charge profiles of the PTI networks cycled at 0.1 A g^{-1} from 1.5 V to 4.5 V in 1 M $LiPF_6$ in EC/DMC electrolyte vs. Li metal. The preparation temperature is indicated in the materials name (in °C). The prefix of the name indicates the long-range order (c – crystalline, a – amorphous) and "d" indicates the material has been copolymerized with 4AP to obtain O and OH moieties as well as extra carbon resulting in a "doped" material.

cycling similar to what would be expected for amorphous carbons (Figure 6). The profiles essentially mimic those of the CTF1 materials suggesting similar mechanisms for charge storage (Figure 7).

In the CTF1 and *bipy*-CTF series, the materials with the highest reversible capacity are amorphous, N-containing porous carbon materials that do not contain well-defined triazine units. In fact, the materials that do contain triazine exhibit very low capacities irrespective of long range order. Therefore, we suggest that the charge storage mechanism does not involve the triazine units.

The inability of triazine to store charge was further confirmed by exploring the electrochemical activity of poly(triazine imide) materials (PTI) which exhibit a high degree of well-defined triazine functionalities. The PTI materials studied here were characterized as described in a previous publication, and the characterization is consistent with the idealized structure of triazine units bridged by imides.[25] The presence of well-defined triazine moieties in these materials despite the high synthesis temperatures is due to the ionothermal synthesis conditions which stabilize the formation of triazine units. Details of the characterization of the materials are presented in the supplementary information. Both amorphous and crystalline PTI materials exhibit negligible electrochemical activity between 1.5 V – 4.5 V (vs. Li) (Figure 8a and b). Doping the amorphous materials by copolymerizing with 4-amino-2,6-dihydroxy pyrimidine (4AP) to obtain O and OH moieties as well as extra carbon results in no significant change in the electrochemical performance (Figure 8c and 8d), although the doped materials work better as photocatalysts.[25] To determine if electrical contact to the active material is the cause of poor capacity, electrode composites were also prepared by ball milling to reduce particle size and increase homogeneity. Ball milling the electrode materials results in even lower capacity (data not shown) likely due to structural damage. Additionally, the impedance spectra of the cells made with PTI materials do not show anomalously high impedance suggesting that conductivity of the electrode is sufficient.

Although the capacity of the PTI materials is very low, they cycle well as evidenced by the stable reversible capacity and high Coulombic efficiency. The c-PTI-600 material exhibits the highest capacity of the PTI networks (Figure 8a), however, all capacities are very low. The capacity is likely due to capacitive storage on the Super P® conductive additive which shows reversible capacities of 3 mA.h g^{-1} in this voltage range. Details on the activity of the Super P® can be found in the supplementary information. It is interesting to note that the PTI materials do exhibit features in the discharge and charge profiles that are absent in the Super P® control suggesting activity of the PTI itself, although with very low capacity. The capacity can be increased by cycling the PTI materials which begin to show plateau-like behavior around 1.5 V (vs. Li) to lower voltages, however, a material operating at 1 V (vs. Li) is no longer a viable cathode alternative. Regardless, by cycling the c-PTI-600 and a-PTI-450 to 1 V (vs. Li), capacities as high as 450 mA.h g^{-1} and 35 mA.h g^{-1} are achieved, respectively. It is important to note that the Super P® conductive carbon contributes to reversible charge storage capacity in this voltage range making it uninformative to normalize the data per mass of active material. Instead, the total mass of the electrode must be considered as active and we find that the capacity of the

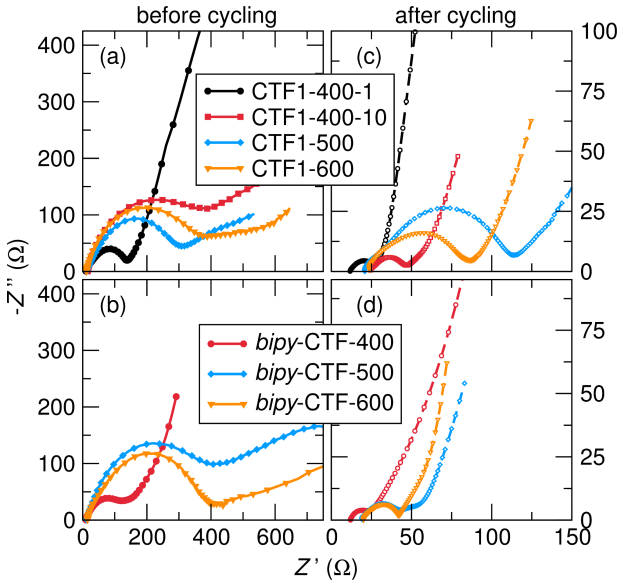

Figure 9. Nyquist plots of the CTF materials before and after cycling at 0.1 A g^{-1} for 100 cycles. The ordered materials, CTF1-400-1 and *bipy*-CCTF-400, exhibit much smaller semicircles indicating lower charge transfer resistance, especially after cycling. Interestingly, these are the materials that also show the lowest capacity.

composite electrodes and the Super P® control exhibit similar capacities when cycled to 1 V (vs. Li) making interpretation of the data difficult. This is discussed in more detail in the supplementary information. It is apparent, however, that the PTI materials do not contribute to better electrochemical performance compared to the conductive carbon additive. The observed capacity is still well below the theoretical capacity of 218 mA.h g^{-1}, assuming a well-defined structure with access to all functional groups and the ability of triazine units to reversibly store one electron per unit, further suggesting that the triazines are inactive. The extremely low capacity of the PTI materials, particularly in the range of cathode materials, suggests that the cell is storing charge by virtue of polarizing the electrodes and double layer storage on the high surface area Super P®. The ordering of the c-PTI-600 network produces channels that can be occupied by interstitial ions,[25] so we expect that these channels also store Li^+. This mechanism could explain the slightly higher capacity and the appearance of broad plateaus in the discharge and charge profiles of the c-PTI-600. The gently sloping charge and discharge profiles of the amorphous PTI materials suggest a capacitive-type charge storage, as mentioned earlier, with minimal Faradaic processes occurring (Figure 8).

With the understanding that charge storage is not occurring at the triazine ring, other material properties that affect the charge storage capabilities were explored in more detail for the CTF1 and *bipy*-CTF networks. Such properties include conductivity, which increases as the preparation temperature increases, and the absence of short range and long range order which facilitates electron transfer. In order to probe the effect of conductivity on the cycling behavior of the CTF materials, the resistances of the cell before and after cycling were evaluated using electrochemical impedance spectroscopy (EIS). We were unable to model the EIS using one consistent equivalent circuit to describe all the Nyquist plots accurately. Instead, here the Nyquist plots are analyzed only in a more qualitative manner. Before cycling, the amorphous materials show wider semicircles indicating larger resistances in the cathode electrode. This suggests that the amorphous materials are more resistive than the low temperature, relatively ordered materials (CTF1-400-1 and *bipy*-CTF-400) since the active material in the cathode is the only variable that changes in the cells before cycling. Interestingly, the materials prepared at higher temperatures also exhibit higher resistances after cycling in both CTF1 and *bipy*-CTF (Figure 9). The wide semicircles in the Nyquist plots after cycling indicate an increase in the charge transfer resistance of the electrodes compared to the charge transfer resistance of the relatively ordered materials after cycling. One reason for the relatively low charge transfer resistance of the CTF1-400-1 and *bipy*-CTF-400 materials could be that the Faradaic reactions occurring at these electrodes produce a SEI which protects the material and allows for good transport. Additionally, CTF1-400-1 and *bipy*-CTF-400 display fewer electrochemical processes that could result in a more pristine material after cycling. We would expect that materials prepared at higher temperatures should show higher conductivity, but we not see a decrease in the charge transfer resistance with increasing temperature of processing. Additionally, the *x*-intercept at high frequencies (low Z') is higher for the materials exhibiting the largest capacities after cycling, which suggests a change in the bulk resistance of the cell (the resistance of the electrode + electrolyte). A change in this high frequency intercept to higher *Z'* is unlikely due to a change in electrolyte resistance and is therefore likely due to a change in the cathode resistance. Therefore, we again observe that the materials showing good electrochemical charge storage have a higher resistance after cycling.

The cycling profiles suggest a purely capacitive mechanism that should show significantly enhanced charge storage capabilities with increased surface area since charge storage occurs only at the interface of the material and the electrolyte. In the CTF materials evaluated here, however, surface area is not the only factor governing the charge storage capabilities. The amorphization of the materials must accompany high surface area in order to see the trends of capacity with surface area (Figure 10b). The capacity also follows a loose trend with the C/N ratio (Figure 10a), however, this could be an artifact since the C/N ratio will undoubtedly increase with increasing preparation temperature.

Another way to determine if the charge storage is capacitive is to evaluate the dependence of the capacity on the cycling rate. Capacitive charge storage shows little rate dependence because there are no kinetically limited charge transfer reactions. The rate limiting step for a capacitor should be the conductivity of the electrolyte, which, for the systems described here, is high because a

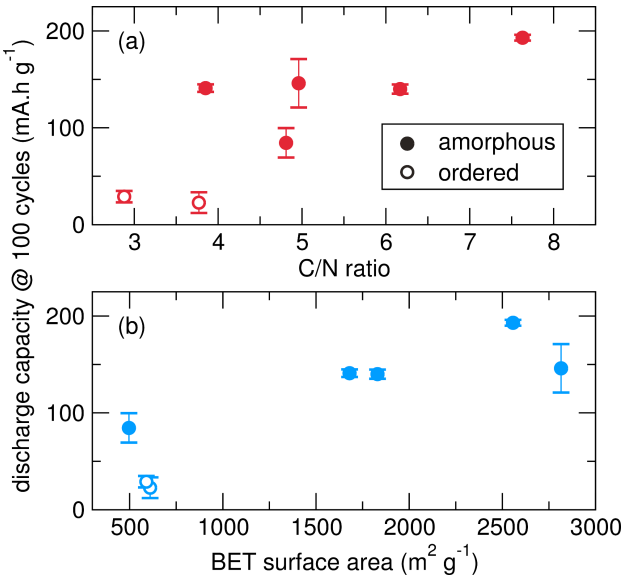

Figure 10. The capacity of the amorphous materials displays a trend with both (a) C/N ratio and (b) BET surface area. The low capacity materials are the CTF1-400-1 and the *bipy*-CTF-400 that both show short range order (evidence of triazine) and are thus labeled as "ordered."

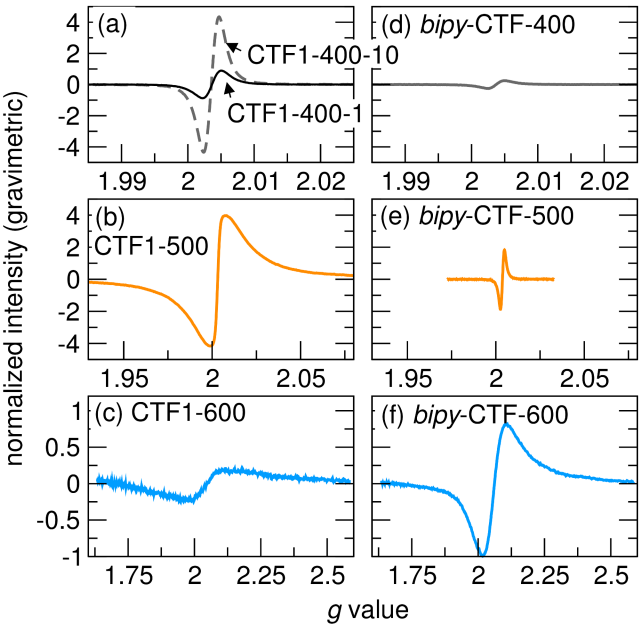

Figure 11. Electron paramagnetic resonance (EPR) spectra of the (a-c) CTF1 and (d-f) *bipy*-CTF materials. All materials show a large quantity of unpaired electrons, however, as the materials are prepared at higher temperatures, the number of unpaired electrons in the materials increase. Additionally, the materials prepared at 600°C (c and f) exhibit a large shift in *g* value suggesting a new environment of the electrons.

1 M supporting electrolyte is used. For a Faradaic material, both the electronic and ionic conductivity of the active material itself can cause rate limitations that are manifested by a strong rate dependence. Indeed, the charge storage capabilities for both the CTF1 and the *bipy*-CTF materials exhibit a slight dependence on rate between 0.1 A/g up to 1.0 A/g. The effect of changing the rate on the capacity is further discussed in the supplementary information. The capacity drops to nearly 0 mA.h g^{-1} when cycled above 5 A g^{-1} which could be due to internal resistance (IR) drops within the cell geometry. At these rates, IR drops within the cell due to insufficient contact of the current collector, etc., can cause loss of capacity. The electrodes are pressed within a Swagelok cell onto a stainless steel current collector and resistances between the electrode powders and the current collector cause this IR drop. This is likely the mechanism for reduced capacity since the slope of the discharge and charge curves are similar but the IR drop is significant as the rates are increased. Regardless, there is some rate dependence from 0.1 A g^{-1} to 0.5 A g^{-1}.

Because the capacity of the CTF1 and *bipy*-CTF materials show a slight rate dependence, the charge storage mechanism may not be purely capacitive. Charge transfer reactions could occur in the materials in addition to surface storage at the interface. However, the charge transfer reactions do not produce any Faradaic plateaus in the discharge and charge profiles. An alternative mechanism that would allow for charge transfer into the material could be the pairing of unpaired electrons in the material. Indeed, the materials showing substantial capacities also contain some concentration of unpaired spins (Figure 11). Furthermore, the PTI materials, which show negligible electrochemical activity, show an EPR response on the order of the background signal of the instrument indicating that they do not contain a considerable measure of unpaired electrons. The symmetric shape of the spectra for the *bipy*-CTF and CTF1 materials indicates that the electrons are relatively localized in the materials, even in the low temperature materials. There is no obvious trend in the number of unpaired spins with the surface area or preparation temperature (Table 2). The materials prepared at 600°C show a shift to higher *g* values suggesting the electrons are in a more electropositive chemical environment (Table 2). This agrees well with the lower N-content of the CTF1-600 and *bipy*-CTF-600 that forces the electrons into a more C-rich environment. Electrons in a more electropositive environment occupy higher energy levels and are thus more easily paired which could be the reason for enhanced cyclability and capacity of CTF1-600 and *bipy*-CTF-600. Ideally we would like to correlate the quantitative spin count in each material to the specific capacity it achieves in the Li half-cell, however, this is a difficult task because the spins in the materials occupy various energy levels and it is unknown if the electrons are fully accessible in the voltage ranges probed here. Therefore, in order to get a more quantitative view, a higher voltage range may need to be used requiring the development of high voltage electrolytes. Due to the high concentration of spins in the materials that exhibit the highest capacities and the odd dependence of capacity on surface area, we suggest that the mechanism for charge storage involves the unpaired electrons in addition to double layer storage, however, the exact mechanism at this point is unclear. A few mechanisms could be at play including pairing of the unpaired spins during discharge

Table 2. Comparison of *g* values and spin counts from the EPR spectra

	g value	Spin count (g^{-1}) x *C**
CTF1-400-1	2.0036	5.7
CTF1-400-10	2.0035	11
CTF1-500	2.0034	3.1
CTF1-600	2.047	2.1
bipy-CTF-400	2.0037	0.7
bipy-CTF-500	2.0037	5.5
bipy-CTF-600	2.061	3.2

* *C* is a constant value for all samples that is dependent on instrument parameters.

or a less direct effect involving the unpaired spins facilitating electron delocalization throughout the material allowing for higher double layer storage. Unpaired spins in organic molecules constitute a high energy species whose excess energy can be lowered by the addition of an electron to form a non-bonded pair (anion) and this can be electrochemically reversible.[14] A similar mechanism can be envisioned for charge storage in the extended networks that are being formed as the CTF materials are prepared at higher temperatures. It is absolutely clear, however, that the stability of the unpaired electrons is not dependent on the presence of triazine moieties.

5. CONCLUSIONS

Several materials prepared from triazine-containing precursors were explored as active materials in Li half cells. Well-defined materials which exhibit strong triazine character show very low gravimetric capacities even if the triazine units are bridged by conjugated moieties, such as phenylene or 2,2'-bypyridine. This directly contradicts the previously suggested bipolar mechanism in which the triazine is n- or p-doped when cycled.[15] In order to achieve high gravimetric capacities, the well-defined conjugated systems must be synthesized at higher temperatures thereby destroying the triazine unit and creating a N-containing amorphous carbon material. These materials have high concentration of localized spins (large numbers of unpaired electrons) that may be involved in the discharge and charge mechanisms. The N-containing amorphous carbon materials are very similar to N-containing porous carbon materials that have been evaluated as supercapacitor materials.[18,21] The capacity of the amorphous materials trends loosely with specific surface area and C/N content. However, higher surface area does not always result in a higher capacity suggesting the mechanism is not purely capacitive. The slight observed rate dependence also suggests a pseudo-capacitive behavior involving charge transfer processes. These charge transfer processes could involve the unpaired electrons in the amorphous materials, and indeed, the inactive PTI materials do not contain unpaired electrons. Suggestions for future work to further probe the charge storage mechanisms involve using in-situ EPR in order to observe the evolution of the spin concentration as a function of discharging and charging.

ASSOCIATED CONTENT

Supporting Information. Experimental details on the preparation and characterization of the PTI materials, elemental analysis of the PTI and CTF materials, Nyquist plots of the PTI cells, capacity as a function of cycle number for the PTI materials, Super P control cells, c-PTI-600 and a-PTI-450 cycled down to 1 V (vs. Li) along with the Super P control cell, differential capacity curves for the CTF materials, GITT of CTF1-400-1 and *bipy*-CTF-400, discharge and charge profiles of *bipy*-CTF-400 cycled down to 1.0 V (vs. Li), and rate dependence of the materials prepared at 500°C. This information is available free of charge via the Internet at http://pubs.acs.org.

AUTHOR INFORMATION

Corresponding Authors

* R. Seshadri, Seshadri@mrl.ucsb.edu
* B. V. Lotsch, B.lotsch@fkf.mpg.de

ACKNOWLEDGMENT

Fellowship support to KAS from the ConvEne IGERT Program of the National Science Foundation (DGE 0801627) is gratefully acknowledged. Experiments at UCSB made use of MRL facilities, supported by the MRSEC Program of the NSF under Grant No. DMR 1121053. KAS and RS gratefully acknowledge useful discussions with Professor Andrew Cooper. MAL is supported by the RISE program through NSF DMR 1121053. SH, KS, and BVL acknowledge financial support by the Max Planck Society, the Deutsche Forschungsgemeinschaft (DFG; SPP-1362, LO 1801/2-1), the Nanosystems Initiative Munich (NIM), the Center for Nanoscience (CeNS) and the Fonds der Chemischen Industrie (FCI). They thank Christian Minke for ssNMR measurements, and Professors Wolfgang Schnick and Thomas Bein for access to measurement facilities.

REFERENCES

(1) Mizushima, K.; Jones, P. C.; Wiseman, P. J.; Goodenough, J. B. Li_xCoO_2 ($0<x\leq1$): A New Cathode Material for Batteries of High Energy Density. *Solid State Ion.* **1981**, *3–4*, 171–174.

(2) Liang, Y.; Tao, Z.; Chen, J. Organic Electrode Materials for Rechargeable Lithium Batteries. *Adv. Energy Mater.* **2012**, *2*, 742–769.

(3) Chen, H.; Armand, M.; Courty, M.; Jiang, M.; Grey, C. P.; Dolhem, F.; Tarascon, J.-M.; Poizot, P. Lithium Salt of Tetrahydroxybenzoquinone: Toward the Development of a Sustainable Li-Ion Battery. *J. Am. Chem. Soc.* **2009**, *131*, 8984–8988.

(4) Williams, D. L.; Byrne, J. J.; Driscoll, J. S. A High Energy Density Lithium/Dichloroisocyanuric Acid Battery System. *J. Electrochem. Soc.* **1969**, *116*, 2–4.

(5) Le Gall, T.; Reiman, K. H.; Grossel, M. C.; Owen, J. R. Poly(2,5-Dihydroxy-1,4-Benzoquinone-3,6-Methylene): A New Organic Polymer as Positive Electrode Material for Rechargeable Lithium Batteries. *J. Power Sources* **2003**, *119–121*, 316–320.

(6) Armand, M.; Grugeon, S.; Vezin, H.; Laruelle, S.; Ribiere, P.; Poizot, P.; Tarascon, J.-M. Conjugated Di-

carboxylate Anodes for Li-Ion Batteries. *Nature Mater.* **2009**, *8*, 120–125.
(7) Walker, W.; Grugeon, S.; Mentre, O.; Laruelle, S.; Tarascon, J.-M.; Wudl, F. Ethoxycarbonyl-Based Organic Electrode for Li-Batteries. *J. Am. Chem. Soc.* **2010**, *132*, 6517–6523.
(8) Liu, M.; Visco, S. J.; Jonghe, L. C. D. Electrochemical Properties of Organic Disulfide/Thiolate Redox Couples. *J. Electrochem. Soc.* **1989**, *136*, 2570–2575.
(9) Visco, S. J.; Liu, M.; Jonghe, L. C. D. Ambient Temperature High-Rate Lithium/Organosulfur Batteries. *J. Electrochem. Soc.* **1990**, *137*, 1191–1192.
(10) Liu, M.; Visco, S. J.; Jonghe, L. C. D. Novel Solid Redox Polymerization Electrodes Electrochemical Properties. *J. Electrochem. Soc.* **1991**, *138*, 1896–1901.
(11) Naoi, K.; Kawase, K.; Mori, M.; Komiyama, M. Electrochemistry of Poly(2,2□-Dithiodianiline): A New Class of High Energy Conducting Polymer Interconnected with S–S Bonds. *J. Electrochem. Soc.* **1997**, *144*, L173–L175.
(12) Naoi, K.; Kawase, K.; Inoue, Y. A New Energy Storage Material: Organosulfur Compounds Based on Multiple Sulfur-Sulfur Bonds. *J. Electrochem. Soc.* **1997**, *144*, L170–L172.
(13) Nakahara, K.; Iwasa, S.; Satoh, M.; Morioka, Y.; Iriyama, J.; Suguro, M.; Hasegawa, E. Rechargeable Batteries with Organic Radical Cathodes. *Chem. Phys. Lett.* **2002**, *359*, 351–354.
(14) Suga, T.; Pu, Y.-J.; Kasatori, S.; Nishide, H. Cathode- and Anode-Active Poly(nitroxylstyrene)s for Rechargeable Batteries:□ P- and N-Type Redox Switching via Substituent Effects. *Macromolecules* **2007**, *40*, 3167–3173.
(15) Sakaushi, K.; Nickerl, G.; Wisser, F. M.; Nishio-Hamane, D.; Hosono, E.; Zhou, H.; Kaskel, S.; Eckert, J. An Energy Storage Principle Using Bipolar Porous Polymeric Frameworks. *Angew. Chem. Int. Ed.* **2012**, *51*, 7850–7854.
(16) Sakaushi, K.; Hosono, E.; Nickerl, G.; Gemming, T.; Zhou, H.; Kaskel, S.; Eckert, J. Aromatic Porous-Honeycomb Electrodes for a Sodium-Organic Energy Storage Device. *Nat. Commun.* **2013**, *4*, 1485.
(17) Sakaushi, K.; Hosono, E.; Nickerl, G.; Zhou, H.; Kaskel, S.; Eckert, J. Bipolar Porous Polymeric Frameworks for Low-Cost, High-Power, Long-Life All-Organic Energy Storage Devices. *J. Power Sources* **2014**, *245*, 553–556.
(18) Hao, L.; Luo, B.; Li, X.; Jin, M.; Fang, Y.; Tang, Z.; Jia, Y.; Liang, M.; Thomas, A.; Yang, J.; et al. Terephthalonitrile-Derived Nitrogen-Rich Networks for High Performance Supercapacitors. *Energy Environ. Sci.* **2012**, *5*, 9747.
(19) Kuhn, P.; Antonietti, M.; Thomas, A. Porous, Covalent Triazine-Based Frameworks Prepared by Ionothermal Synthesis. *Angew. Chem. Int. Ed.* **2008**, *47*, 3450–3453.
(20) Hug, S.; Tauchert, M. E.; Li, S.; Pachmayr, U. E.; Lotsch, B. V. A Functional Triazine Framework Based on N-Heterocyclic Building Blocks. *J. Mater. Chem.* **2012**, *22*, 13956–13964.
(21) Zhang, Z. J.; Cui, P.; Chen, X. Y. Structure and Capacitive Performance of Porous Carbons Derived from Terephthalic Acid–Zinc Complex via a Template Carbonization Process. *Ind. Eng. Chem. Res.* **2013**, *52*, 16211–16219.
(22) Jiang, J.-X.; Su, F.; Trewin, A.; Wood, C. D.; Niu, H.; Jones, J. T. A.; Khimyak, Y. Z.; Cooper, A. I. Synthetic Control of the Pore Dimension and Surface Area in Conjugated Microporous Polymer and Copolymer Networks. *J. Am. Chem. Soc.* **2008**, *130*, 7710–7720.
(23) Aurbach, D.; Markovsky, B.; Weissman, I.; Levi, E.; Ein-Eli, Y. On the Correlation between Surface Chemistry and Performance of Graphite Negative Electrodes for Li Ion Batteries. *Electrochim. Acta* **1999**, *45*, 67–86.
(24) Novák, P.; Joho, F.; Imhof, R.; Panitz, J.-C.; Haas, O. In Situ Investigation of the Interaction between Graphite and Electrolyte Solutions. *J. Power Sources* **1999**, *81–82*, 212–216.
(25) Schwinghammer, K.; Tuffy, B.; Mesch, M. B.; Wirnhier, E.; Martineau, C.; Taulelle, F.; Schnick, W.; Senker, J.; Lotsch, B. V. Triazine-Based Carbon Nitrides for Visible-Light-Driven Hydrogen Evolution. *Angew. Chem. Int. Ed.* **2013**, *52*, 2435–2439.

Table of Contents artwork

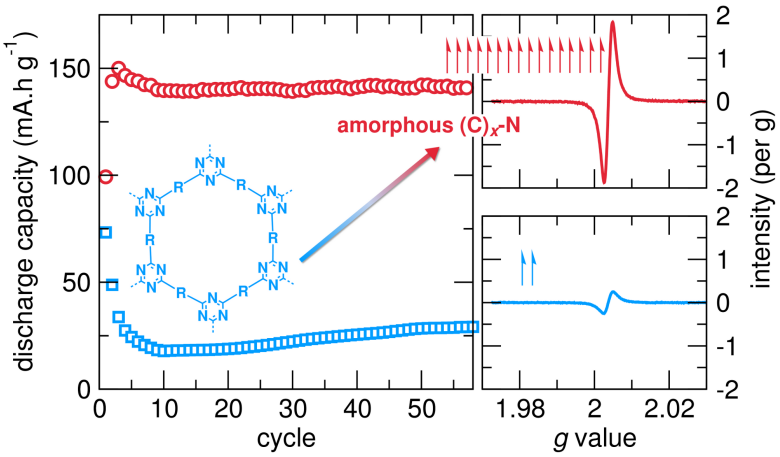

An investigation of the charge storage capabilities of a series of organic networks that contain triazine moieties or are derived from triazine-containing precursors reveals that charge storage does not occur at the triazine unit, and instead is capacitive, and may be facilitated by unpaired spins.

Supporting Information: Lithium charge storage mechanisms of cross-linked triazine networks and their porous carbon derivatives

Kimberly A. See,[†,‡] Stephan Hug,[§,^,ℌ] Katharina Schwinghammer,[§,^,ℌ] Margaret A. Lumley,[‡,∥] Yonghao Zheng,[∇] Jaya M. Nolt,[∥] Galen D. Stucky,[†,‡,∇] Fred Wudl,[∇] Bettina V. Lotsch,[*,§,^,ℌ] Ram Seshadri[*,†,‡,∥,∇]

[†]Mitsubishi Chemical – Center for Advanced Materials, University of California, Santa Barbara, CA 93106, USA
[‡]Department of Chemistry and Biochemistry, University of California, Santa Barbara, CA 93106, USA
[ℌ]Nanosystems Initiative Munich and Center for Nanoscience, Schellingstr. 4, 80799 München, Germany
[§]Department Chemie, Ludwig-Maximilans-Universität München, Butenandtstr. 5-13, 81377 München, Germany
[^]Max-Planck-Institut für Festkörperforschung, Heisenbergstr. 1, 70569 Stuttgart, Germany
[∥]Materials Research Laboratory, University of California, Santa Barbara, CA 93106, USA
[∇]Materials Department, University of California, Santa Barbara, CA 93106, USA.

Preparation conditions and characterization of the PTI materials

The preparation of crystalline PTI (c-PTI) was first reported by Bojdys et al. via an ionothermal method.[1] Detailed characterization of the PTI materials determined that they consist of a 2D network of planar triazine units bridged by imides with the channels filled by Li^+ and Cl^-.[2] Long range order in the PTI materials can be modulated by varying the preparation procedure to produce amorphous PTI materials (a-PTI) which show no evidence of long range order in the X-ray diffraction (XRD) patterns.[3] It is known that a-PTI synthesized above 450°C outperforms c-PTI as a photocatalyst suggesting that their electronic structures also change according to the morphology.[3] For this reason, both amorphous and crystalline PTI networks were evaluated as potential battery materials.

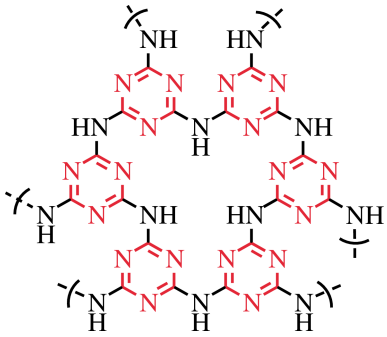

Figure S1. Poly(triazine imide), or PTI, is composed of 1,3,5-triazine bridged by secondary amines. These materials are well-defined with Li^+ and Cl^- ions occupying the channels (not shown). The N in the triazine or imide can be substituted, or "doped", with O or C depending on the synthesis procedure.

Both c-PTI and a–PTI materials were prepared for analysis in Li batteries. The synthesis of the c-PTI materials was performed according to previously published procedures.[1,2] Dicyandiamide (0.20 g, 2.38 mmol) and an eutectic mixture of lithium chloride (59.2 mol%, 0.90 g, 21.3 mmol) and potassium chloride (40.8 mol%, 1.01 g, 14.7 mmol) were hand ground with a mortar and pestle in a glove box. The reaction mixture was transferred in a dried quartz glass vessel, placed in a horizontal tube furnace, and heated under atmospheric Ar pressure at 6°C min^{-1} to 400°C. This temperature was held for 12 h and then cooled to room temperature at 20°C min^{-1}. The resulting powders were then re-ground in Ar and transferred to a dried, thick-walled fused silica tube (15 mm OD and 11 mm ID) which was then evacuated and sealed at a length of 120 mm. The sealed ampoule was placed in a horizontal tube furnace and heated at 1°C min^{-1} to 600°C in a second heating step and held at 600°C for 24 h. After cooling to room temperature (6°C min^{-1}), the ampoule was broken and the sample was isolated and washed several times with boiling water to remove residual salt. The resulting material c-PTI was obtained as a brown powder (80 mg, 50%).

The synthesis of a-PTI and "doped" a-PTI (a-d-PTI), made by copolymerizing 4-amino-2,6-dihydroxy pyrimidine (4AP) with a-PTI, was carried out according to previous work by our group.[3] "Doped" here indicates that some of the N in the triazine or imide moieties are replaced by C or O. Dicyandiamide (0.50 g, 5.95 mmol) and an eutectic mixture of lithium chloride (59.2 mol%) and potassium chloride (40.8 mol%) were ground together in an Ar glove box. In the case of the copolymerized a-d-PTI samples, 4AP (0.72 g, 0.86 mmol) was added to the reaction mixture before grinding. The starting mixtures were transferred in a quartz glass vessel which was heated in a horizontal Ar-purged tube furnace at 12°C min^{-1} to the target temperature (indicated in Table 1). The temperature was held for 6 hr. followed by cooling to room

temperature (20°C min^{-1}). The resulting powders were ground to achieve a homogenous product and heated again under the same conditions. Finally, the samples were isolated and washed several times with boiling water to remove residual salts. a-PTI yielded a yellow powder (0.15 g, 38%) and in the case of a-d-PTI-550, a dark orange colored product (0.16 g, 40%) was recovered.

The FTIR spectra clearly show strong signatures of the 1,3,5-triazine functionality indicating that well-defined triazine units are intact in the final materials at all synthesis temperatures.[3] The ratio of C to N in this family of materials is the lowest for all materials discussed here (Table S1). The crystalline PTI materials, denoted c-PTI, exhibit sharp reflections in the XRD indicative of long range order. The amorphous PTI materials, denoted a-PTI, show no long range order in the XRD except layer stacking. This family of materials provides structures with well-defined triazine frameworks and varying long range order.

Table S1. Summary of synthesis conditions for poly(triazine imide) materials.

	Copolymerized ("doped") with 4AP	Syn. Temp (°C)
c-PTI-600	no	600
a-PTI-450	no	450
a-d-PTI-500	yes	500
a-d-PTI-550	yes	550

Table S2. Elemental analysis of the poly(triazine imide) and covalent triazine frameworks.

	N (wt%)	C (wt%)	H (wt%)	C/N (molar ratio)
c-PTI-600	46.8	29.8	1.5	0.74
a-PTI-450	55.1	26.7	4.3	0.56
a-d-PTI-500	44.8	28.8	2.8	0.75
a-d-PTI-550	41.6	29.3	2.6	0.82
CTF1-400-1	18.60	70.20	3.30	4.4
CTF1-400-10	14.63	70.34	3.62	5.6
CTF1-500	12.39	76.45	1.34	7.2
CTF1-600	10.37	79.16	1.34	5.3
bipy-CTF-400	20.42	58.85	4.08	3.3
bipy-CTF-500	16.42	63.14	2.67	4.5
bipy-CTF-600	13.61	67.53	2.01	5.8

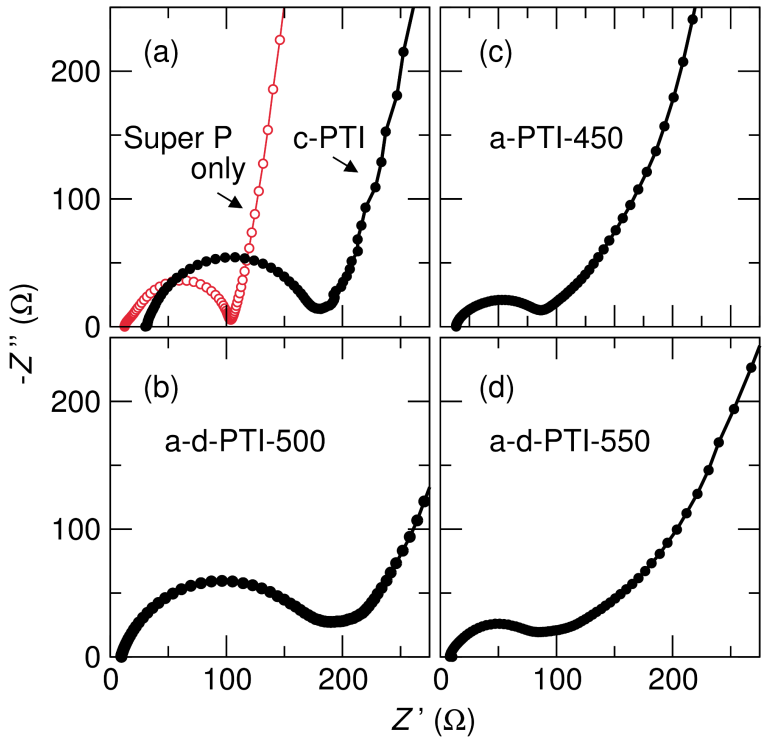

Figure S2. The Nyquist plots of the PTI cells before cycling do not show anomalously high resistances suggesting that the electrode conductivity does not limit capacity. The plot of a Super P only cell is shown in (a) for reference.

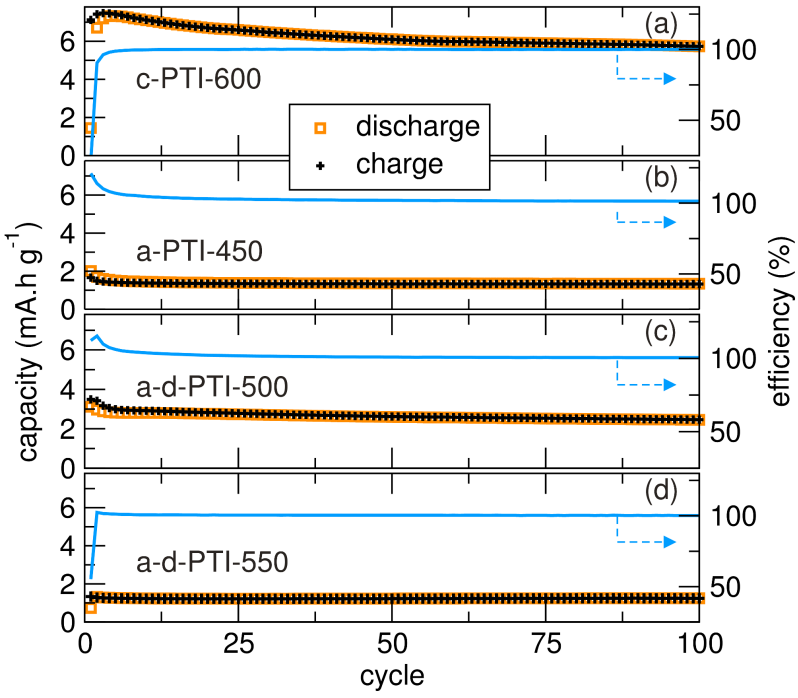

Figure S3. The PTI networks show very low capacities when cycled at 0.1 A g^{-1} from 1.5 V to 4.5 V in 1 M $LiPF_6$ in EC/DMC electrolyte vs. Li metal. (a) The c-PTI-600 material exhibits slightly higher capacities than the amorphous materials (a-PTI and a-d-PTI) synthesized at (b) 450 °C, (c) 500 °C, and (d) 550 °C.

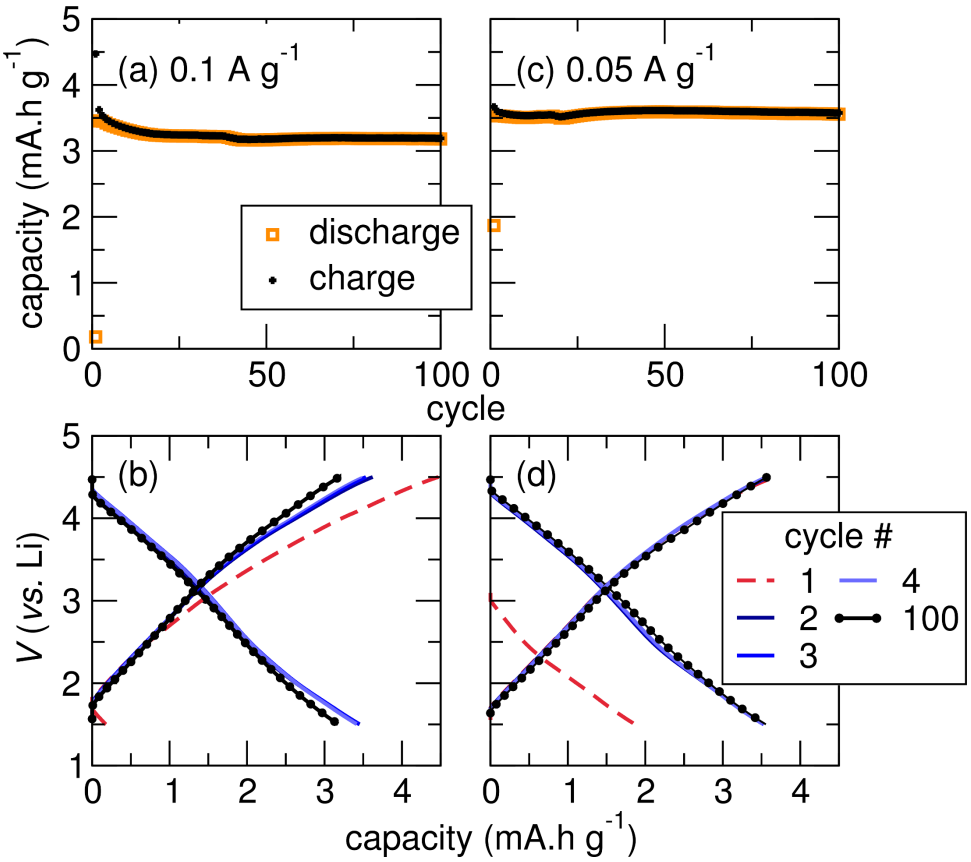

Figure S4. Control cells cycled with only the conductive carbon additive Super P (5 mg) at 0.1 A g^{-1} (left column) and 0.05 A g^{-1} (right column) from 1.5 V (*vs.* Li) to 4.5 V (*vs.* Li). (a) The capacity of the Super P only cells is below 5 mA.h g^{-1} when cycled at 0.1 A g^{-1}. (b) The profiles are indicative of capacitive storage through double layer interactions only. (c) The capacity is also very low when cycled at 0.05 A g^{-1}, suggesting minimal rate dependence. (d) Again, these cells exhibit capacitive-like behavior as would be expected.

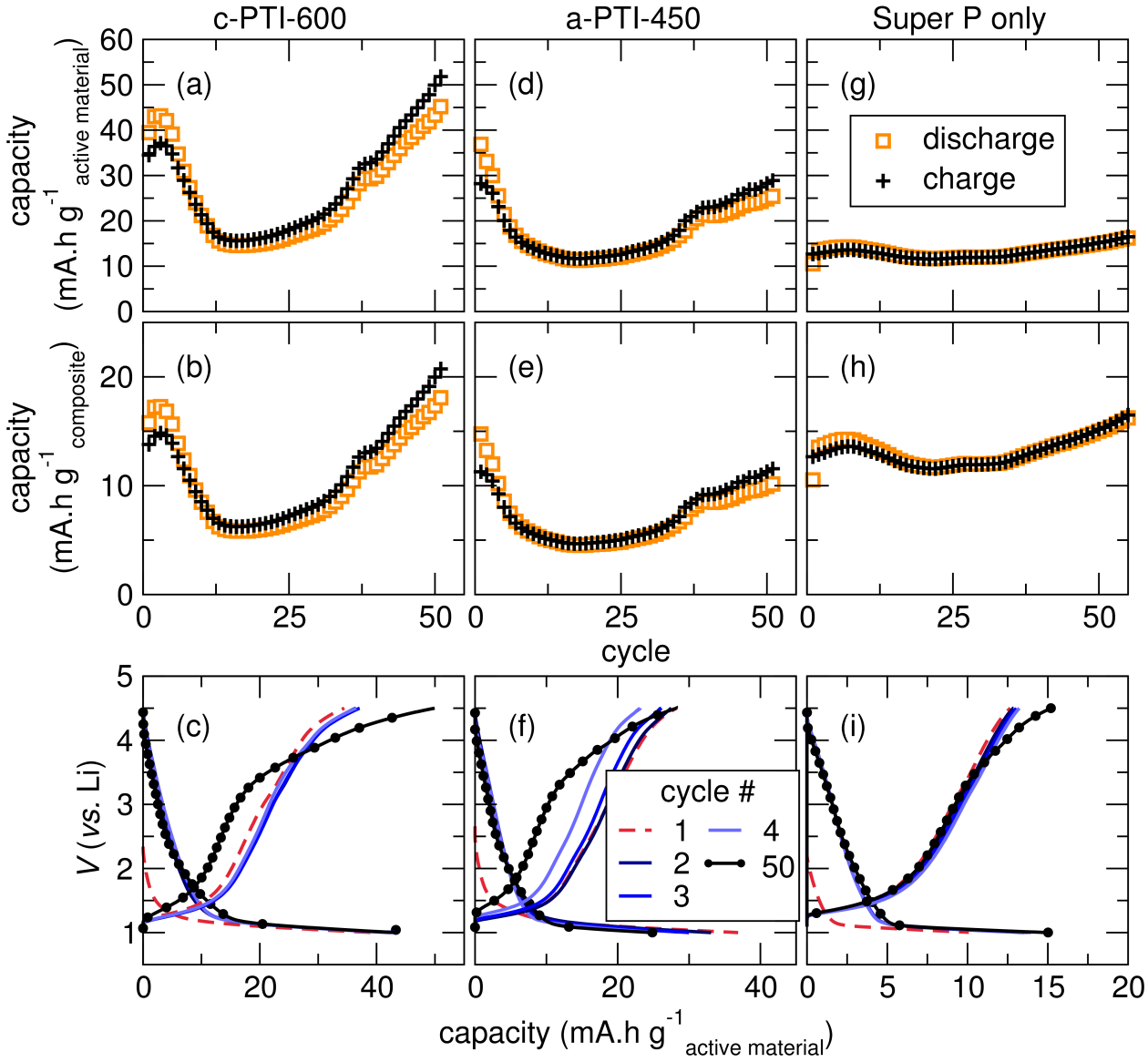

Figure S5. Galvanostatic cycling at 0.1 A g^{-1} of (a-c) c-PTI-600 and (d-f) a-PTI-450 from 1 V (*vs.* Li) to 4.5 V (*vs.* Li) along with the (g-i) Super P control cell. The two PTI materials that show promising plateaus near the end of discharge when cycled to 1.5 V (*vs.* Li) exhibit apparent capacity increases when cycled to 1.0 V (vs. Li) (top row). The capacity of c-PTI-600 increases from < 7 mA.h g^{-1} to (a) > 40 mA.h g^{-1} over 50 cycles. (c) The discharge and charge profiles of the c-PTI-600 exhibit reversible plateaus. (d) The capacity of a-PTI-450 also increases once it is cycled to lower voltages and exhibits a similar dip in the capacity at lower cycle numbers. (f) The profiles of the a-PTI-450 are similar to those of the c-PTI-600. (g) Because these cells were cycled to lower voltages, it is important to consider the activity of the carbon additive. The Super P control cell exhibits substantial reversible capacity in this voltage range, as well, contributing to the capacities seen in (a) and (d). (i) The discharge curve of Super P closely resembles those of the (c) c-PTI-600 and (f) a-PTI-450. Because of the activity of Super P at these potentials, it is only meaningful to consider the capacity normalized to the total mass of the electrode and compare it to the control cell, as shown in (b), (e), and (h). In this case, all three systems are relatively similar suggesting that the c-PTI-600 and a-PTI-450 do not contribute any substantial capacity to the Super P electrode.

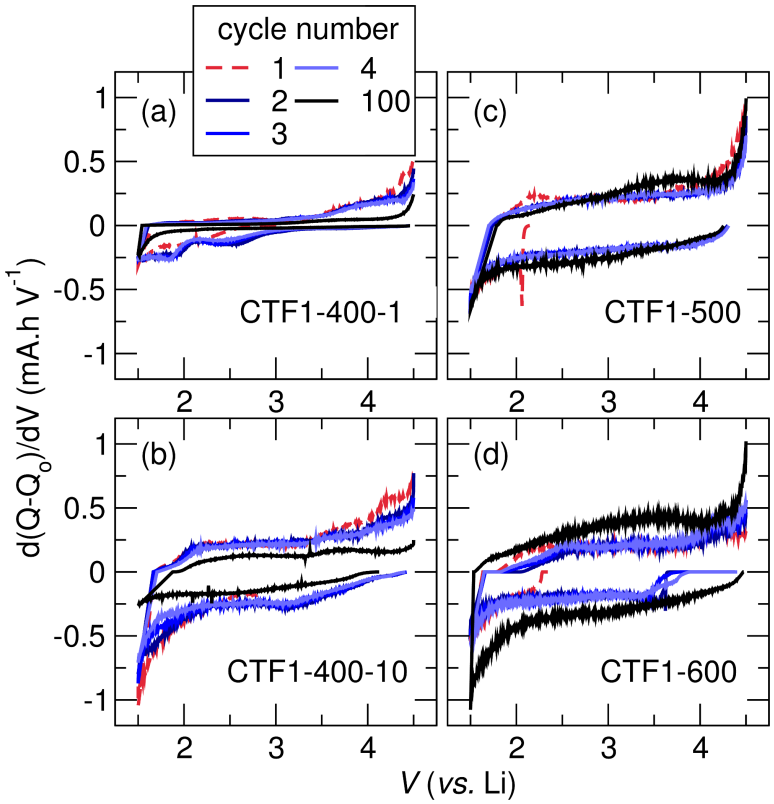

Figure S6. Differential capacity curves of the CTF1 materials cycled at 0.1 A g^{-1} from 1.5 V to 4.5 V (*vs.* Li) in 1 M $LiPF_6$ EC/DMC. (a) CTF1-400-1 shows two very broad peaks around 2.75 V (*vs.* Li) and 2.0 V (*vs.* Li) in the initial cycles suggesting the presence of two phase regions in the initial cycling, however, the capacity is very low. (b-d) The amorphous materials exhibit curves suggestive of capacitive mechanisms absent of any peaks.

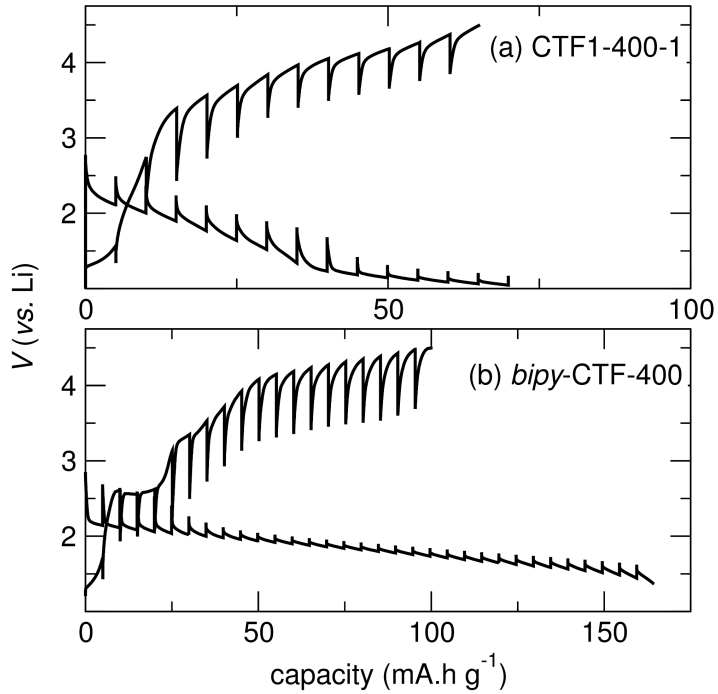

Figure S7. Galvanostatic intermittent titration technique (GITT) of the low temperature, rigid CTF networks showing the near-equilibrium discharge and charge profiles. (a) The discharge and charge profiles of the CTF1-400-1 exhibit a similar shape to those of the cell cycled at 0.1 A g^{-1} (Figure 4a) suggesting no kinetically limited processes are occurring. (b) The *bipy*-CTF-400 material exhibits a similar plateau in the discharge and charge as seen in the 0.1 A g^{-1} cycled cell (Figure 7a).

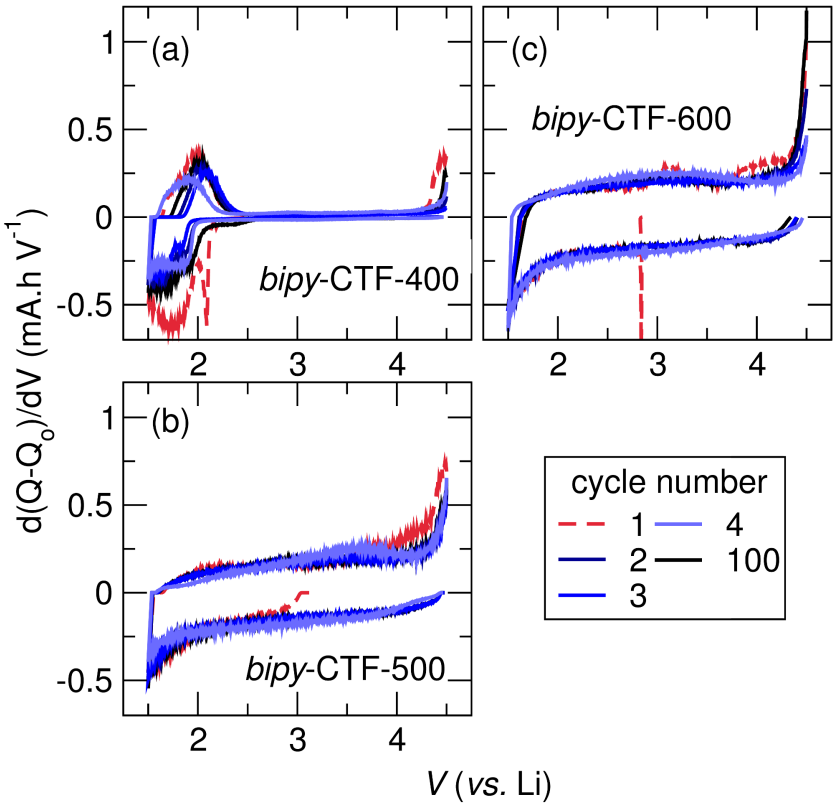

Figure S8. Differential capacity curves of the *bipy*-CTF materials cycled at 0.1 A g^{-1} from 1.5 V to 4.5 V (*vs.* Li) in 1 M $LiPF_6$ EC/DMC. The only material exhibiting peaks characteristic of two-phase regions is (a) *bipy*-CTF-400. (b-c) The amorphous materials exhibit open curves characteristic of capacitive charge storage.

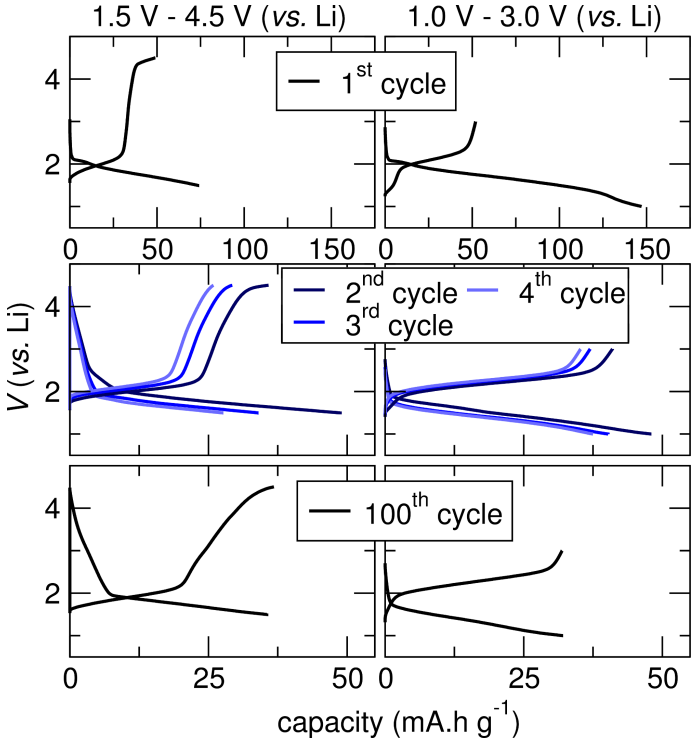

Figure S9. The discharge and charge profiles of *bipy*-CTF-400 when cycled between (left column) 1,5 V – 4.5 V (*vs.* Li) and (right column) 1.0 V – 3.0 V (*vs.* Li). All cells are cycled at 0.1 A g^{-1}. Decreasing the discharge cutoff voltage does not increase the capacity after the 1st cycle suggesting irreversible Faradaic processes are occurring below 1.5 V.

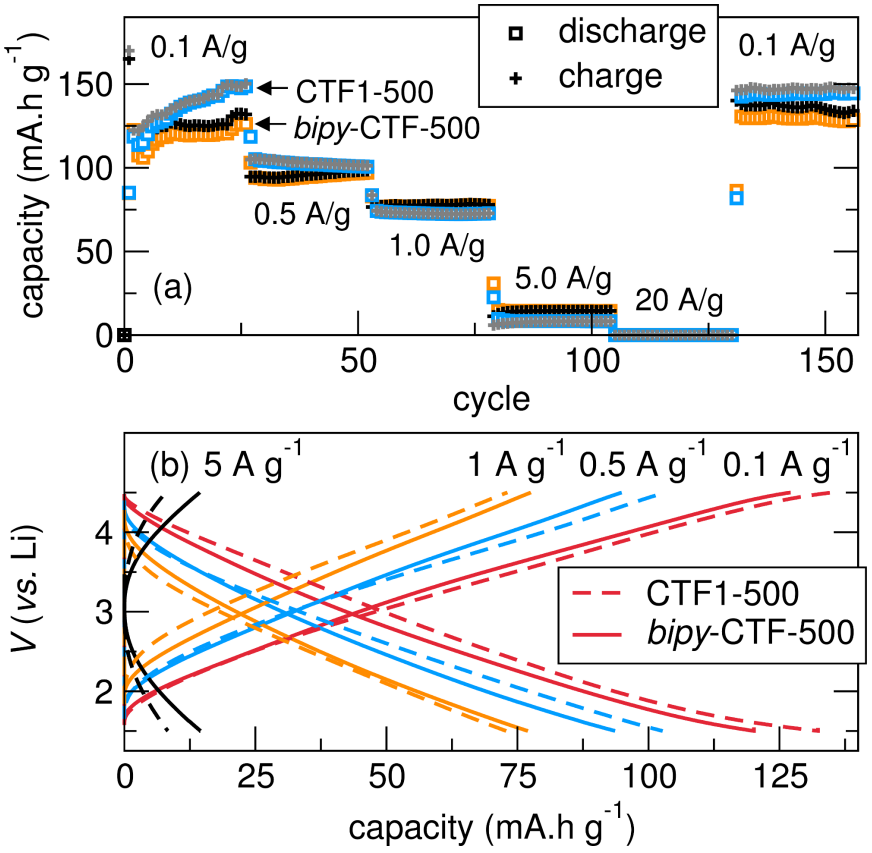

Figure S10. (a) The charge storage capabilities of CTF1 and *bipy*-CTF materials prepared at 500 °C show a dependence on the rate suggesting a kinetically limited process. (b) The discharge and charge profiles exhibit large internal resistance drops when cycled at higher rates suggesting that the cell configuration is causing the lowered capacity.

References

(1) Bojdys, M. J.; Müller, J.-O.; Antonietti, M.; Thomas, A. Ionothermal Synthesis of Crystalline, Condensed, Graphitic Carbon Nitride. *Chem. – Eur. J.* **2008**, *14* (27), 8177–8182.

(2) Wirnhier, E.; Döblinger, M.; Gunzelmann, D.; Senker, J.; Lotsch, B. V.; Schnick, W. Poly(triazine Imide) with Intercalation of Lithium and Chloride Ions $[(C_3N_3)_2(NH_xLi_{1-x})_3 \cdot LiCl]$: A Crystalline 2D Carbon Nitride Network. *Chem. – Eur. J.* **2011**, *17* (11), 3213–3221.

(3) Schwinghammer, K.; Tuffy, B.; Mesch, M. B.; Wirnhier, E.; Martineau, C.; Taulelle, F.; Schnick, W.; Senker, J.; Lotsch, B. V. Triazine-Based Carbon Nitrides for Visible-Light-Driven Hydrogen Evolution. *Angew. Chem. Int. Ed.* **2013**, *52* (9), 2435–2439.